Modelling chromospheric line profiles as diagnostics of velocity fields in ω Centauri red giant stars

M. Vieytes[1], P. Mauas[1][*], C. Cacciari[2][**], L. Origlia[2] and E. Pancino[2,]

[1] Instituto de Astronomía y Física del Espacio, Universidad de Buenos Aires, Argentina
e-mail: `mariela@iafe.uba.ar, pablo@iafe.uba.ar`

[2] INAF - Osservatorio Astronomico, Via Ranzani 1, 40127 Bologna, Italy
e-mail: `carla.cacciari@oabo.inaf.it, livia.origlia@oabo.inaf.it, elena.pancino@oabo.inaf.it`

ABSTRACT

Context. Mass loss of ∼ 0.1-0.3 $M_\odot$ from Population II red giant stars (RGB) is a requirement of stellar evolution theory in order to account for several observational evidences in globular clusters.

Aims. The aim of this study is to detect the presence of outward velocity fields, which are indicative of mass outflow, in six luminous red giant stars of the stellar cluster ω Cen.

Methods. We compare synthetic line profiles computed using relevant model chromospheres to observed profiles of the Hα and Ca II K lines. The spectra were taken with UVES (R=45,000) and the stars were selected so that three of them belong to the metal-rich population and three to the metal-poor population, and sample as far down as 1 to 2.5 magnitudes fainter than the respective RGB tips.

Results. We do indeed reveal the presence of low-velocity outward motions in four of our six targets, without any apparent correlation with astrophysical parameters.

Conclusions. This provides direct evidence that outward velocity fields and mass motions exist in RGB stars as much as 2.5 mag fainter than the tip. On the assumption that the mass outflow may eventually lead to mass loss from the star, we estimate mass-loss rates of some 10^{-9}-$10^{-10} M_\odot$ yr^{-1} that are compatible with the stellar evolution requirements. These rates seem to be correlated with luminosity rather than metallicity.

Key words. line: profiles; – globular clusters: individual (ω Cen); – stars: atmospheres; – stars: mass loss; – stars: Population II; – techniques: spectroscopic

1. Introduction

Mass loss of ∼ 0.1-0.3 $M_\odot$ from Population II red giant branch (RGB) stars is a requirement of stellar evolution theory in order to account for observational evidence in globular clusters (GCs) such as i) the very existence of the horizontal branch (HB) and its morphology, ii) the pulsational properties of RR Lyrae stars, iii) the absence of asymptotic giant branch (AGB) stars brighter than the red giant branch (RGB) tip, and the chemistry and characteristics in the AGB, post-AGB and planetary nebula evolutionary phases, iv) the mass of white dwarf (WD) stars (Castellani & Renzini 1968; Rood 1973; Fusi Pecci et al. 1993; D'Cruz et al. 1996; Kalirai et al. 2007). In addition, mass loss significantly affects other areas of astrophysics, for example the UV excess in elliptical galaxies and the interaction between the cool intracluster medium and hot halo gas.

The few tens of solar masses lost by RGB stars should accumulate in the central regions of GCs, especially of the more massive ones, without the sweeping mechanisms between Galactic plane crossings. However, no conclusive evidence was found for a significant presence of any form (neutral or ionized gas, dust) of intracluster matter, even in some of the clusters that would be most likely to accumulate the material lost from cluster stars (Smith et al. 1990; Origlia et al. 1997; Freire et al. 2001). The advent of the *Spitzer Space Telescope* has triggered a more accurate search for cold dust within GCs. Eight Galactic GCs were observed and again only upper limits were found, which is well below expectations for dust production from mass loss in cluster RGB and AGB stars (Barmby et al. 2009, and references therein). The only exception is NGC 7078 (M15) which shows high signal-to-noise evidence for an IR excess and hence dusty intracluster medium in the core (Evans et al. 2003; Boyer et al. 2006), and possibly ω Cen if the four dust clouds that were detected in the field are confirmed to be intracluster material that is in the process of escaping from the cluster (Boyer et al. 2008). This implies that either dust production from mass loss is less efficient, or that the mechanisms able to remove the intracluster material are more efficient than commonly believed.

An alternative and complementary approach is to study the mass loss phenomenon where it occurs, namely on the RGB stars themselves, by detecting either outflow motions in the outer region of the stellar atmospheres or the presence of circumstellar envelopes at larger distances (typically tens/hundreds of stellar radii).

The latter approach, which needs the use of IR data, was first made possible by mid-IR photometry taken from the ground (Frogel & Elias 1988) and with the IRAS satellite (Gillet et al. 1988; Origlia et al. 1996), and a decade later by new observa-

---

tions from the ISOCAM onboard ISO. A deep survey on six massive Galactic GCs with ISOCAM data revealed an infrared excess, which is indicative of dusty circumstellar envelopes, in ~ 15% of the RGB (or AGB) stars in the ~ 0.7 mag brightest interval ($M_{bol} \leq -2.5$) (Origlia et al. 2002, and references therein). A more accurate survey in 17 Galactic GCs was made possible recently by the use of data from the IRAC onboard *Spitzer* (Fabbri et al. 2008). The results from this survey on about 100 stars in 47 Tuc (Origlia et al. 2007, 2010) show unambiguously that mid-IR excess radiation caused by dust is present along the RGB down to about the level of the HB and is correlated with luminosity. Mass-loss rates were derived for these stars, allowing to define the first empirical mass-loss formula calibrated on Population II stars. The dependence on luminosity of this mass-loss rate is considerably shallower than the widely used Reimers law (Reimers 1975a,b) and the formulation by Catelan (2000) which were both calibrated on Population I red giants. We refer the reader to Origlia (2008) for a review.

Other *Spitzer*-based studies available on 47 Tuc (Boyer et al. 2010), ω Cen (Boyer et al. 2008; Mc-Donald et al. 2009), M15 (Boyer et al. 2006), and NGC 362 (Boyer et al. 2009) find that mass loss is confined near the tip of the RGB, and occurs mostly in AGB or variable stars, with the exception of M15 where a population of dusty red giants has been detected. These conclusions, however, were revised by Origlia et al. (2010) in 47 Tuc where the use of a better dust indicator allowed them to detect dust at fainter magnitudes along the RGB.

The other approach, aiming at detecting velocity fields and outward motions in the stellar chromospheres, has also been the subject of several studies since the late 70's. This is the approach we adopt in the present study, as described in detail in the following sections.

2. Diagnostics of velocity fields

The pioneering investigations of the Hα line profile in globular cluster red giants (Cohen 1976,1978, 1979, 1980, 1981; Mallia & Pagel 1978; Peterson 1981, 1982; Cacciari & Freeman 1983; Gratton et. al 1984) detected asymmetric and variable Hα emission wings along the brightest part of the RGB, which were generally interpreted as evidence of an extended atmosphere until Dupree et al. (1984) showed that they could instead be signatures of a static stellar chromosphere.

Therefore, the attention shifted to *asymmetry* and *coreshift* in chromospheric line profiles as possible indicators of mass motions. This approach was applied to the Na I D and Ca II K lines in addition to Hα, in both globular cluster RGB stars (Peterson 1981; Bates et al. 1990, 1993; Dupree et al. 1994; Lyons et al. 1996; Cacciari et al. 2004; Mészáros et al. 2008, 2009a) and in metal-poor field red giants (Smith et al. 1992; Dupree & Smith 1995). Blueshifted (outward) velocity core shifts were detected in several cases, all of them much smaller than the escape velocity from the stellar photosphere. Better results were obtained using the Mg II $\lambda2800$ *h* and *k* lines which form higher in the atmosphere. These data are only available for few bright metal-poor field or globular cluster red giants (Dupree et al. 1990a,b, 1994; Smith & Dupree 1998), and indeed allowed the detection of stellar winds with terminal speeds exceeding the escape velocities, from which mass-loss rates of about 10^{-11} to 10^{-9} $M_{\odot}$ yr^{-1} were estimated.

The infrared He I $\lambda10830$ line, which forms still higher in the atmosphere than optical or near-UV chromospheric lines, has been proposed to probe the outer regions of the atmosphere where the wind begins to accelerate (Dupree et al. 1992; Smith et

al. 2004). In a recent study of 41 metal-poor field giants, Dupree et al. (2009) detected fast outflows of material, in about 40% of cases fast enough to escape from the star. From their model chromosphere and the analysis of line strength and outflow speed they derived mass loss rates in the range ~ 10^{-10} to 10^{-8} $M_{\odot}$ yr^{-1}, which provide the amount of mass loss (~ 0.2 $M_{\odot}$) needed by stellar evolution models during the RGB and RHB phases. However, as they point out, helium lines can be strongly affected by X-ray photoionization of He, as was shown for the Sun by Mauas et al. (2005) and Andretta et al. (2008).

In any case, this potentially interesting method can be presently applied only to bright (i.e. field) stars, given the difficulty of obtaining high-resolution high S/N spectra in the near IR. Therefore, the use of the optical spectroscopic diagnostics can still provide important information, and it may well be the only viable option to study the much fainter RGB stars in globular clusters, at least until powerful high-resolution IR spectrographs become widely available.

The advantage of monitoring the mass-loss phenomenon in globular cluster RGB stars is the convenience of studying a sample with the same metallicity and distance within each cluster, and therefore the possibility to detect with relatively good accuracy the dependence of the mass-loss phenomenon on luminosity (within a given cluster) and on chemical abundance (by comparing results from different clusters). This was the aim of the most recent studies, which used detailed and custom-tailored chromospheric model calculations to fit the whole profile of chromospheric lines in RGB stars of a few globular clusters. Mauas et al. (2006, hereinafter Paper I) studied the Ca II K and the Hα line in RGB stars in NGC2808, and Mészáros et al. (2009b) modelled Hα for RGB stars in M13, M15 and M92. Although some dependence on luminosity, temperature, and metallicity can be seen, the possible transient occurrence of the mass loss phenomenon produces considerable uncertainty in the final results.

The aim of the present study is to compare the kinematical structure of the chromosphere, i.e. the presence and intensity of a velocity field, in a few metal-rich and metal-poor stars with similar characteristics in all other respects, to derive an estimate of the mass-loss rate and highlight a possible effect of metallicity on the mass-loss phenomenon. A comparison is also made with our previous study on the metal-intermediate globular cluster NGC 2808.

The stellar system ω Cen is the ideal place for this test, as it contains multiple stellar populations with different metallicities.

3. The data

For this study we selected three metal-rich and three metal-poor red giant stars from the extensive sample studied by Pancino (2003, hereafter P03) (see Table 1 and Fig. 1). The selected stars have bolometric magnitudes between 1 and 2.5 fainter than the RGB tip.

All data were obtained as part of a large observational programme for the detailed study of the ω Cen sub-populations (P03; Pancino et al. 2004; Ferraro et al. 2004; Sollima et al. 2005a,b).

The visual BVI photometry was taken with the WFI at the 2.2m ESO-MPI telescope (La Silla, Chile) by P03. Infrared photometry was taken with SOFI at the ESO NTT (La Silla, Chile) for the initial study of these stars (P03, Sollima et al. 2004), but in the present analysis we used JK data from the 2MASS database. The photometric data are listed in Table 1.

The spectroscopic data were taken in April 2001 with UVES in slit mode (R~45,000) at the VLT (ESO-Chile), sampling si-

Table 1. Programme RGB stars in ω Cen: photometric parameters. Coordinates and JK photometry are taken from the 2MASS database, visual photometry is from P03.

Star	LEID	RA	DEC	B	V	I	J	K
ROA159	33011	13 25 17.5	-47 24 26.6	13.24	11.98	10.45	9.537	8.715
ROA256	41039	13 25 53.8	-47 28 12.2	13.53	12.28	10.97	9.977	9.190
ROA238	37247	13 27 02.4	-47 26 06.0	13.61	12.44	11.15	10.191	9.363
WFI321293	42042	13 26 03.8	-47 28 32.8	14.96	13.69	12.41	11.286	10.448
ROA523	48321	13 27 04.8	-47 31 01.3	14.74	13.39	11.93	10.678	9.732
WFI140419	32149	13 27 14.5	-47 23 51.2	14.83	13.49	12.11	10.960	10.072

Table 2. Programme RGB stars in ω Cen: physical parameters. The parameters in columns 2-5 are taken from P03 (the notation *mp* for ROA256 means *metal poor*), and BC_K are derived from P03 temperatures and the calibration by Montegriffo et al. (1998). For the expansion velocities and mass outflow rates in columns 11 and 12 see Sect. 5.1.

Star	[Fe/H]	[Ca/H]	T_{eff} ± 100 K	$\log g$ ± 0.2 dex	BC_K	M_{bol}	$\log L/L_{\odot}$	$R/R_{\odot}$	$M/M_{\odot}$	V_{exp} (km s^{-1})	$\dot{M}$ ($M_{\odot}$ yr^{-1})
ROA159	-1.72[1]	-1.37	4200	0.9	2.386	-2.64	2.952	56	0.88	5	1.1 10^{-9}
ROA256	-1.71[1]	mp	4300	1.1	2.316	-2.23	2.788	45	0.87	15	6.0 10^{-9}
ROA238	-1.80[1]	-1.34	4200	1.2	2.386	-1.99	2.692	42	0.90	15	3.2 10^{-9}
WFI321293	-0.72	-0.35	4200	1.6	2.386	-0.90	2.256	25	0.87	...	...
ROA523	-0.65	-0.25	4200	1.4	2.386	-1.62	2.544	35	1.14	40	5.0 10^{-10}
WFI140419	-0.68	-0.34	4200	1.5	2.386	-1.28	2.408	30	1.05	...	...

Note: [1] - these values are from Cayrel de Strobel et al. (2001).
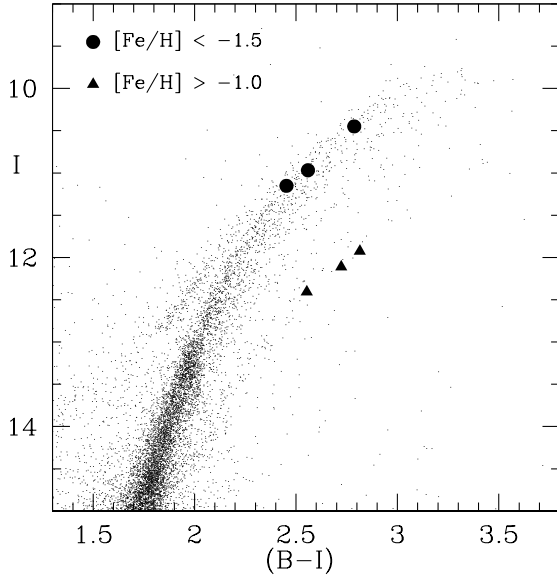
Fig. 1. I,(B–I) colour-magnitude diagram of ω Cen showing the RGB: the six targets of the present study are plotted as big filled circles (metal poor) and big filled triangles (metal rich).

3.0.1. Atmospheric parameters

The values of metallicity, effective temperature, and gravity listed in Table 2 (columns 2-5) are taken from P03, who derived initial values from the available multiband photometry and further refined them through the detailed abundance analysis of the relevant Fe I and Fe II lines. The three metal-poor stars are also included in the high-resolution study by Cayrel de Strobel et al. (2001), who derived very similar values of metallicity, effective temperature, and gravity. On the contrary, the low-resolution spectral survey by van Loon et al. (2007) produced significantly different results for the four stars that are in common with the present study (i.e. ROA159, ROA523, WFI321293 and WFI140419), but the value of that work lies in its statistical power rather than in the accuracy of the individual estimates.

For a consistency check we estimated the temperatures also from the J-K colours using the temperature scale and calibration by Montegriffo et al. (1998), and assuming for ω Cen a reddening E(B-V)=0.11 mag from Lub (2002), and the relations E(J-K)=0.52E(B-V) and A_K=0.36E(B-V) from Cardelli et al. (1989). The results are very close to those of P03 within the errors of these determinations (typically ± 100 K). Therefore we used the P03 temperature values to estimate the K bolometric corrections BC_K from the calibration by Montegriffo et al. (1998). The luminosities were then derived from the K magnitudes assuming for ω Cen a distance modulus (m-M)$_0$=13.70 ± 0.10 mag (Cacciari et al. 2006), and for the Sun $M_{bol}(\odot)$=4.74 mag.

The stellar radii are obtained from the basic equation of stellar structure

$$\log R/R_{\odot} = 0.5 \log L/L_{\odot} - 2\log T_{eff} + 7.522$$

multaneously the spectral ranges 350-460 nm (Ca II H-K) and 580-700 nm (Hα) with S/N ~ 100/px. The spectra were reduced with the optimal extraction procedure of the UVES pipeline.

and the values of mass are estimated from the relation

$$logM/M_\odot = logL/L_\odot + logg - 4logT_{eff} + 10.607$$

. The typical mass for these stars is about 0.8-0.9 $M_\odot$ from stellar evolution theory, and indeed the values we obtain agree well considering the errors associated to the temperature and gravity estimates.

The values of the above-mentioned physical parameters are listed in Table 2.

4. The model chromospheres

To build our models, we adopted mean values of log(g) = 1.5, and metallicities [Fe/H]=-0.67 for the metal-rich stars. For the metal-poor stars we used log(g) = 1. and [Fe/H]=-1.6. In both cases we adopted a value of [α/Fe]=+0.3. These values are in line with those listed in Table 2.

For each group of stars we used as a starting point the photospheric models computed by Kurucz (2005)[1] with the closest set of parameters to those of the observed stars. For the metal-rich stars we used the model corresponding to T_{eff} = 4250 K, log(g)=1.5, and [Fe/H] = -0.5, and for the metal-poor stars the model with T_{eff} = 4250 K, log(g)=1 and [Fe/H] = -1.5. We point out that once we adopted a given temperature *vs.* metallicity distribution, we recomputed the densities and all atomic populations *ab initio*.

On top of the photospheric model, we superimposed a chromospheric rise. We initially tried models similar to the ones used in Paper I, with T increasing linearly with negative log(m), where m is the mass column density. However, we found that we needed to increase T faster just above T_{min} and form a chromospheric plateau to reproduce the Ca II K profiles. Although these models are therefore much more complex than the ones in Paper I, they resemble more closely those usually used for dwarf stars and, in particular, for the Sun.

Upon the chromosphere, we added a "transition region" where the temperature rises abruptly up to 1.5×10^5 K, to assure convergence of the calculations. The structure of this "transition region" has no influence on the computed profiles.

Since the asymmetries observed are not very large, they can be considered as a second order change in the line profiles. Furthermore, calculations including velocity fields take much longer to compute. Therefore, we first found a reasonable agreement between the computed profiles and the observed ones, and then we included a velocity field to reproduce the asymmetries. We modified this velocity field until a satisfactory match between observed and computed profiles was found. The advantage of this approach is that the velocities are not "measured" from the profiles, but modelled self-consistently along with the rest of the atmospheric parameters, and the region corresponding to each value of the velocity field is well-determined, unlike for other methods such as the bisector.

For every T vs. log(m) distribution we used the programme Pandora (Avrett & Loeser 1984) to solve the non-LTE radiative transfer and the statistical and hydrostatic equilibrium equations, assuming turbulent velocities varying from 2 to 20 km s^{-1}. We self-consistently computed non-LTE populations for 10 levels of H (for details on the atomic models, see Falchi & Mauas 2002), 13 of He I (Mauas et al. 2005), 9 of C I (Mauas, Avrett & Loeser 1989), 15 of Fe I, 8 of Si I (Cincunegui & Mauas 2001), 8 of Ca I and Na I, 6 of Al I (Mauas, Fernández Borda & Luoni 2002),

and 7 of Mg I (Mauas, Avrett & Loeser 1988). In addition, we computed 6 levels of He II and Mg II, and 5 of Ca II. We also self-consistently computed the contribution to the opacity of the most abundant molecule, CO (Mauas et al. 1990).
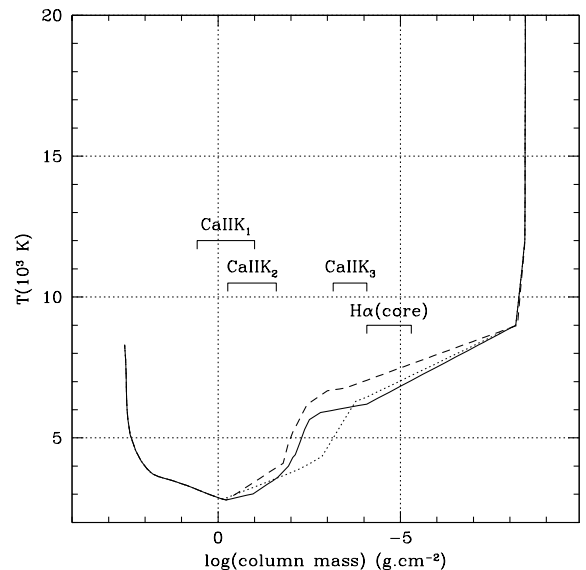
Fig. 2. Our chromospheric models for the metal-rich stars: ROA 523 (solid line), WFI 140419 (dotted line) and WFI 321923 (dashed line). The approximate depth of formation of the Hα core and of the Ca II K_1, K_2 and K_3 line components are also indicated.

For every species considered we included all bound-free transitions and the most important bound-bound transitions. Ly-α, the Ca II H and K, and Mg II h and k lines were all computed with a full partial-redistribution treatment (Falchi & Mauas 1998, for a discussion).

In our calculations we assumed a plane-parallel atmosphere, for simplicity. However, once the final model was obtained, we computed the emitted profiles assuming a spherically symmetric atmosphere, and we found no significant changes in the emitted profiles with respect to the plane-parallel approximation.

5. Analysis and results

In Fig. 2 we show the atmospheric models for the metal-rich stars with the depth of formation of the lines we used as diagnostics. The depth of formation is defined as the depth where most of the observed photons are formed. The models for the metal-poor stars are shown in Fig. 3. The velocities that give the best fit with the observed line asymmetries are plotted in Fig. 4. For two of the metal-rich stars, WFI 140419 and WFI 321293, the observed profiles are symmetric, and we therefore did not need to include any velocities to reproduce them.

The computed Hα and Ca II K line profiles are compared with the observations in Fig. 5. The observed profiles have been normalized to the continuum emission implied by Kurucz's model, and shifted by a quantity corresponding to the individual stellar radial velocity to move the profiles to their rest wavelengths.

One can see in the figure that the agreement between computed and observed profiles is quite good. In Paper I, the com-

---

[1] Kurucz, R.L., 2005, http://kurucz.harvard.edu/grids.html
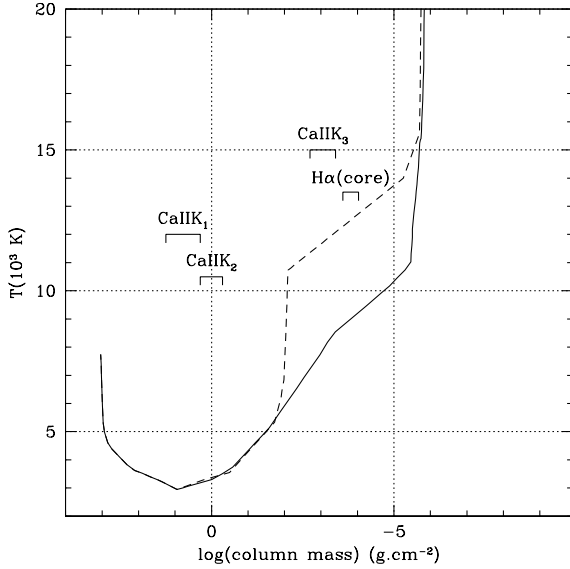
Fig. 3. Same as Fig. 2 for the metal-poor stars: ROA159 (dashed line), ROA238 and ROA256 (solid line).
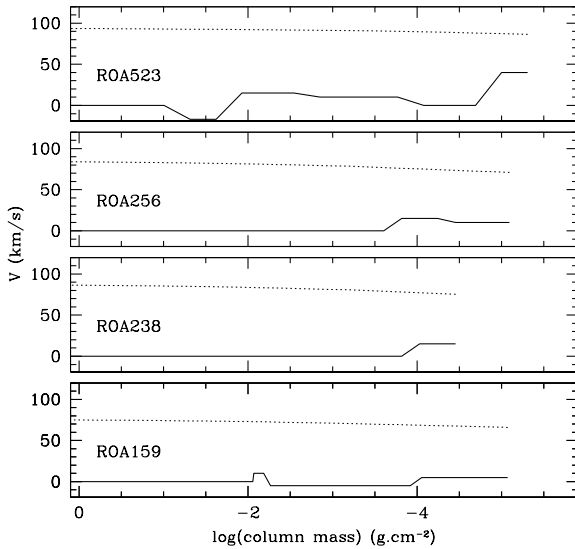
Fig. 4. Velocity as a function of depth (solid line) for the metal-rich star ROA523 (top panel) and the three metal-poor stars (lower panels). A positive velocity implies outflow. No velocity fields were required for the two metal-rich stars WFI321293 and WFI140419, which are therefore not shown in this plot. The velocities were derived from the best match with the Ca K and Hα lines and are compared to the corresponding escape velocity (dotted line).

puted Hα profiles were broader and slightly deeper in the line core than the observed ones. However, this discrepancy is much smaller in the present models.

Regarding the Ca II profiles, they are much noisier and are therefore more difficult to interpret. In a couple of cases, the models produced higher K_3 central intensities than the observed profiles, as was generally the case in Paper I. As we discussed in

that paper, this can be due to the assumption of a homogeneous chromosphere, since any contribution of a pure photospheric line should be noticed mainly in the line centre. We do not expect a significant contribution of interstellar Ca, since we do not see evidence of it in our spectra, and it could contribute to the Ca II core profile only if the velocity of the interstellar medium were similar to that of the cluster (~ 230 km s^{-1}).

However, on average the match to the observations given by these models is better than the one we found in Paper I. This can be because these stars show lower velocities, and in only one case there is a noticeable emission in the Hα wings. On the other hand, this may also be because these models are much more complex, since here we did not require a linear T vs. log(m).

Regarding the models, there is a large difference between those for the metal-rich and metal-poor stars, with the latter ones starting at smaller column masses. On the other hand, the three models for the metal-rich stars agree with each other. Indeed, the computed profiles for these stars are unaffected by the structure of the regions above log(m)= 10^{-7} (see Fig. 2), and we therefore used similar structures for each model in that region.

For the metal-poor stars, the model for ROA238 and ROA256 is the same, and the profiles differ only because of different velocity fields. The model for ROA159 is much hotter. This is reflected in the emission wings in the Hα profile, which, as in the models of Paper I, is a direct sign of a steep chromospheric temperature rise.

5.1. Velocity fields and mass loss

In general, the stars studied here have smaller velocity fields than those modelled in Paper I. Furthermore, in two cases (WFI140419 and WFI321293), we did not need to include velocities to fit the observations. For the other stars, we show the full velocity field in Fig. 4. For comparison, we also show the corresponding escape velocity at each height Z from the centre of the star, computed as $V_{esc}=620$ (M/Z)$^{1/2}$, where Z and the stellar mass M are in solar units, and the velocity is in km s^{-1}. We assumed a typical mass M=0.85 $M_\odot$ for all stars.

The Hα line core is the feature that forms higher up in the atmosphere, so we can only infer the velocity up to the height where it is formed, about 20-30% of a stellar radius above the photosphere. All metal-poor stars show low expansion velocities (≤ 15 km s^{-1}) at the most external point, and only the metal-rich ROA523 has a high expansion velocity (40 km s^{-1}). These values are similar to those obtained in Paper I. However, since the gravities of the present targets are 5-10 times larger than those in Paper I, the escape velocities are higher too and we cannot be certain that the material above this level is indeed escaping from the atmosphere.

However, there is a mass outflow at this height, which can be estimated using the simple formulation

$$\dot{M} = 1.3 \times m_H \times N_H \times 4\pi \times R^2 \times V$$

,

where m_H and N_H are the mass and the density of hydrogen atoms, R the distance from the stellar centre, and V the velocity of the outermost layer for which we have a determination. The factor 1.3 takes care of the helium abundance Y=0.23. The expansion velocities detected in the outermost part of the atmosphere where the Hα core forms are shown in Table 2, as well as the mass outflow rates calculated from the above equation.

As there are no signs of a reversal in the velocity field, *i.e.* there is no material falling back in, the most probable situation is
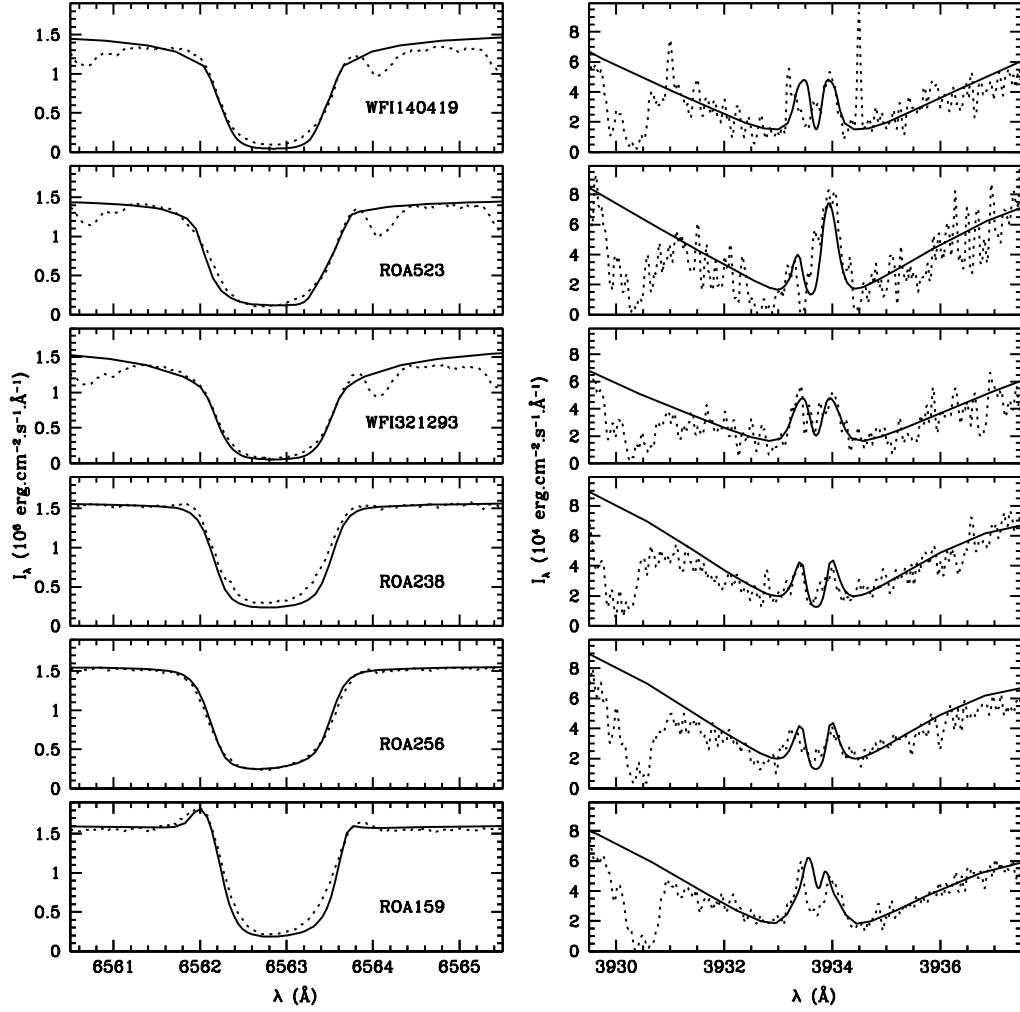
Fig. 5. For every star, the observed profiles (dotted lines) are compared with the synthetic profiles computed with the velocity fields shown in Figs. 4 (solid lines). The profiles for Hα (left panel) and Ca II K (right panel) for the metal-rich stars are shown in the three uppermost panels, and those for the metal-poor stars in the three lowermost ones.

that the velocity continues to increase with distance, until eventually it reaches the escape velocity which, of course, is decreasing with distance.

5.2. Energy requirements

To estimate the energy requirements to sustain the chromosphere, *i.e.* to constrain the possible heating mechanisms at work, we compute the radiative cooling rate Φ (erg cm^{-3} s^{-1}), namely the net amount of energy radiated at a given depth by the atmosphere, which is given by

$$\Phi = 4\pi \int \kappa_\nu \, (S_\nu - J_\nu) \, d\nu$$

.

A positive value implies a net loss of energy (cooling), and a negative value represents a net energy absorption (heating).

In this study we compute the contributions due to H$^-$, H, He I, Mg I and II, Ca I and II, Fe I, Si I, Na I, Al I, and CO. The

overall results and the most important individual contributions for the model that represents star ROA523 are presented in Fig. 6. We do not include the rates for the other models, which are very similar.

The main difference with the results obtained for other stars (e.g. in Paper I) is the presence of a negative region in the mid-chromosphere, caused by backwarming by Ly-α emission, which has its origin in a more external layer. In the rest of the atmosphere, these rates are similar to those obtained in Paper I. As we pointed out there, the energy required is much lower for giant stars than for dwarf stars of similar T$_{eff}$ (Mauas et al. 1997; Vieytes et al. 2005, 2009). Indeed, the cooling rate reaches up to 10^{-4} erg cm^{-3} s^{-1} for these giant stars, 5 orders of magnitude smaller than for the dwarfs. On the other hand, the energy *per particle* is of the same order of magnitude, since the particle density is also 5 orders of magnitude smaller for the present stars.

As in the models in Paper I, the cooling rate in the coolest parts of the atmosphere is negative and due almost entirely to

H^-, as was already noted for dwarf stars. However, almost all cooling in that region is due to CO, which is the only molecule included in the calculations. Because at these low temperatures the presence of other molecules should be expected, it is reasonable to expect that the inclusion of other molecular species in the calculations should bring the atmosphere closer to radiative balance.

In the mid- and high-chromosphere the energy balance is determined essentially by the hydrogen cooling rate. This is of course more important for the metal-poor stars, where the influences of cooling by metallic lines such as the Mg II and Ca II can be neglected.
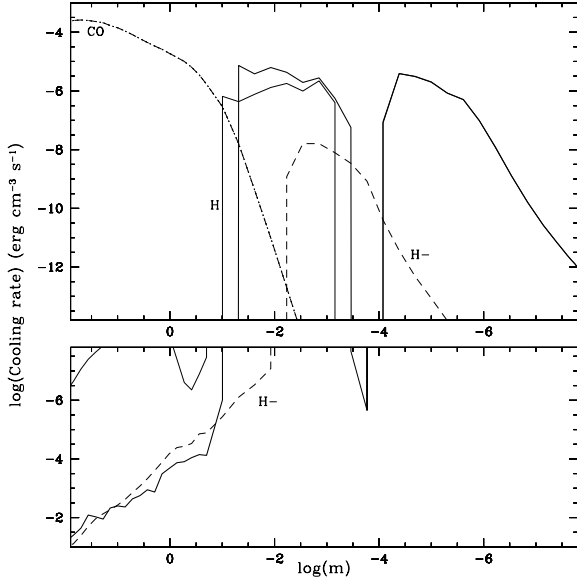
Fig. 6. LogΦ, *i.e.* the total net radiative cooling rate, as a function of depth for our model for the star ROA523 (thick line), and the most important contributions to it. In the upper panel we show positive values (*i.e.* net cooling), and in the lower panel we show negative values (*i.e.* net heating).

6. Summary and conclusions

We studied three metal-rich and three metal-poor red giant stars in the stellar cluster ω Cen. To analyse in detail and characterize the possible outward velocity fields that are indicative of mass outflow, we built model chromospheres and computed synthetic line profiles that we compared with high-resolution profiles of the Hα and Ca II K lines, unlike Mészáros et al. (2009b), who only used Hα.

We can summarize our results as follows:

– As we noticed in Paper I, the existence of emission in the Ca II K lines is of chromospheric origin and does not require the presence of a velocity field. This is also true for the Hα line. However, a fairly steep rise in temperature with log(m) is needed to explain this emission, as can be seen in the model for ROA159.

– On the other hand, the asymmetries in the Ca II K and Hα line profiles indicate the presence of velocity fields in four out of six stars. These "expansion" velocities are less than

about 15 km s^{-1} except for ROA523, where it reaches about 40 km s^{-1}, they are all outward and provide clear evidence that some mass outflow occurs in these stars.

– The only metal-rich star showing outward velocity and mass outflow is ROA523, the brightest of its group. On the other hand, all the metal-poor stars are brighter than the metal-rich ones, and show evidence of outward velocities and slightly higher values of mass outflow rates. This suggests that there is a stronger correlation of the mass loss phenomenon with luminosity rather than with metallicity, as found in several previous studies (see Sect. 1).

– On the assumption that the mass outflow eventually escapes the star, the rates of mass loss are estimated as a few 10^{-9}-10^{-10} M$_\odot$ yr^{-1}, in general agreement with previous estimates from the Mg II k line (Dupree et al. 1990a,b, 1994; Smith & Dupree 1998) and with the requirements of the stellar evolution theory.

– In Paper I we obtained a similar result, namely four stars with low outward velocity (less than 20 km s^{-1}) and one with a velocity of about 50 km s^{-1}. The globular cluster NGC 2808 has [Fe/H] $\sim$ -1.15, which is intermediate between the two populations studied here, and all stars studied in Paper I have $logL/L_\odot > 3.0$ and somewhat larger radii than the present targets. The mass-loss rates estimated in Paper I are quite similar to the present ones, supporting the suggestion that a higher luminosity could favour mass loss. However, the likely transient nature of the mass-loss phenomenon may contribute to mask any correlation with metallicity and luminosity.

– As in Paper I, the energy per unit volume required to sustain the chromosphere is much smaller than the energy needed for a dwarf star with similar T$_{eff}$. However, the energy *per particle* is of similar amount.

As a final conclusion, this study provides additional evidence that outward velocity fields and mass motions exist along the RGB at fainter levels (i.e. as much as 2.5 mag) than the RGB tip, as already suggested by Origlia et al. (2010) based on evidence for "historic" mass loss from dust emission in 47 Tuc.

References

Andretta, V., Mauas, P. J. D., Falchi, A. & Teriaca, L. 2008, ApJ, 681, 650
Avrett E.H., & Loeser R., 1984, in *Methods in Radiative Transfer*, ed. W. Kalkofen, Cambridge, Univ. Press, p. 341.
Barmby, P., Boyer, M.L., Woodward, C.E., Gehrz, R.D., van Loon, J.Th., Fazio, G.G., Marengo, M. & Polomski, E. 2009, AJ, 137, 207
Bates, B., Catney, M.G. & Keenan, F.P. 1990, MNRAS, 245, 238
Bates, B., Kemp, S.N. & Montgomery, A.S. 1993, A&AS, 97, 937
Boyer, M. L., Woodward, C. E., van Loon, J. Th., Gordon, K. D., Evans, A., Gehrz, R. D., Helton, L. A., & Polomski, E. F. 2006, AJ, 132, 1415
Boyer, M. L., McDonald, I., van Loon, J.Th., Woodward, C. E., Gehrz, R. D., Evans, A. & Dupree, A.K. 2008, AJ, 135, 1395
Boyer, M. L., McDonald, I., van Loon, J.Th., Gordon, K.D. et al. 2009, ApJ, 705, 746
Boyer, M. L., van Loon, J. Th., McDonald, I. et al. 2010, ApJ, 711, L99
Cacciari, C. & Freeman, K.C. 1983, ApJ, 268, 185
Cacciari, C., Bragaglia, A., Rossetti, E. et al. 2004, A&A, 413, 343
Cacciari, C., Sollima, A. & Ferraro, F.R. 2006, Mem. Soc. Astron. Italiana, 77, 245
Cardelli, J.A., Clayton, G.C. & Mathis, J.S. 1989, ApJ, 345, 245
Castellani, V. & Renzini, A. 1968, Ap&SS, 2, 310
Catelan, M. 2000, ApJ, 531, 826

Cayrel de Strobel, G., Soubiran, C. & Ralite, N. 2001, A&A, 373, 159
Cincunegui, C. & Mauas, P.J.D. 2001, ApJ 552, 877
Cohen, J.G. 1976, ApJ, 203, L127
Cohen, J.G. 1978, ApJ, 223, 487
Cohen, J.G. 1979, ApJ, 231, 751
Cohen, J.G. 1980, ApJ, 241, 981
Cohen, J.G. 1981, ApJ, 247, 869
D'Cruz, N.L., Dorman, B., Rood, R.T. & O'Connell, R.W. 1996, ApJ, 466, 359
Dupree, A.K., Hartmann, L. & Avrett, E.H. 1984, ApJ, 281, L37
Dupree, A.K., Harper, G.M., Hartmann, L., Jordan, C., Rodgers, A.K. & Smith, G.H. 1990a, ApJ, 361, L9
Dupree, A.K., Hartmann, L. & Smith, G.H. 1990b, ApJ, 353, 623
Dupree, A.K., Sasselov, D.D & Lester, J.B. 1992, ApJ, 387, L85
Dupree, A.K., Hartmann, L., Smith, G.H., Rodgers, A.W., Roberts, W.H. & Zucker, D.B. 1994, ApJ, 421, 542
Dupree, A.K. & Smith, G.H. 1995, AJ, 110, 405
Dupree, A.K., Smith, G.H. & Strader, J. 2009, AJ, 138, 1485
Evans, A., Stickel, M., van Loon, J.Th., Eyres, S.P.S., Hopwood, M.E.L. & Penny, A.J. 2003, A&A, 408, L9
Fabbri, S., Origlia, L., Rood, R.T., Ferraro, F.R., Fusi Pecci, F. & Rich, M. 2008, Mem. S.A.It. Vol. 79, 720
Falchi, A. & Mauas, P.J. 1998, A&A, 336, 281
Falchi, A. & Mauas, P.J. 2002, A&A, 387, 678
Ferraro, F.R., Sollima, A., Pancino, E., Bellazzini, M., Straniero, O., Origlia, L. & Cool, A.M. 2004, ApJ, 603, L81
Freire, P.C., Kramer, M., Lyne, A.G., Camilo, F., Manchester, R.N. & D'Amico, N. 2001, ApJ, 557, 105
Frogel, J.A. & Elias, J.H. 1988, ApJ, 324, 823
Fusi Pecci, F., Ferraro, F.R., Bellazzini, M., Djorgovski, G.S., Piotto, G. & Buonanno, R. 1993, AJ, 105, 1145
Gillet, F.C., deJong, T., Neugebauer, G., Rice, W.L. & Emerson, J.P. 1988, AJ, 96, 116
Gratton, R.G., Pilachowski, C.A. & Sneden, C. 1984, A&A, 132, 11
Kalirai, J.S., Bergeron, P., Hansen, B.M.S., Kelson, D.D., Reitzel, D.B., Rich, R.M. & Richer, H.B. 2007, ApJ, 671, 748
van Loon, J.Th., van Leeuwen, F., Smalley, B., Smith, A.W., Lyons, N.A., McDonald, I. & Boyer, M.L. 2007, MNRAS, 382, 1353
Lub, J. 2002, in "Omega Centauri, a unique window into Astrophysics", ASP Conf. Ser. 265, 95
Lyons, M.A., Kemp, S.N., Bates, B. & Shaw, C.R. 1996, MNRAS, 280, 835
Mallia, E.A. &; Pagel, B.E. 1978, MNRAS, 184, 55P
Mauas, P.J.D., Avrett, E.H. & Loeser, R. 1988, ApJ, 330, 1008.
Mauas, P.J.D., Avrett, E.H. & Loeser, R. 1989, ApJ, 345, 1104
Mauas, P.J.D., Avrett, E.H. & Loeser, R. 1990, ApJ, 357, 279
Mauas, P. J. D., Falchi, A., Pasquini, L., & Pallavicini, R. 1997, A&A, 326, 249
Mauas, P.J.D., Fernández Borda, R. & Luoni, M.L. 2002, ApJS, 142, 285
Mauas, P.J.D., Andretta, V., Falchi, A.,Falciani, R., Teriaca, L. & Cauzzi, G. 2005, ApJ, 619, 604
Mauas, P.J.D., Cacciari, C. & Pasquini, L. 2006, A&A, 454, 609 (Paper I)
McDonald, I., van Loon, J.Th., Decin, L., Boyer, M.L., Dupree, A,.K., Evans, A., Gehrz, R.D. & Woodward, C.E. 2009, MNRAS, 394, 831
Mészáros, Sz., Dupree, A.K., & Szentgyorgyi, A.H. 2008, AJ, 135, 1117
Mészáros, Sz., Dupree, A.K., & Szalai, T. 2009a, AJ, 137, 4282
Mészáros, Sz., Avrett, E.H. & Dupree, A.K. 2009b, AJ, 138, 615
Montegriffo, P., Ferraro, F.R., Origlia, L. & Fusi Pecci, F. 1998, MNRAS, 297, 872
Origlia, L., Ferraro, F.R. & Fusi Pecci, F. 1996, MNRAS, 280, 572
Origlia, L., Scaltriti, F., Anderlucci, E., Ferraro, F.R. & Fusi Pecci, F. 1997, MNRAS, 292, 753
Origlia, L., Ferraro, F.R., Fusi Pecci, F. & Rood, R.T. 2002, ApJ, 571, 458
Origlia, L., Rood, R.T., Fabbri, S., Ferraro, F.R., Fusi Pecci, F. & Rich, R.M. 2007, ApJ, 667, 85
Origlia, L. 2008, Mem. Soc. Astron. Italiana, 79, 432
Origlia, L., Rood, R.T., Fabbri, S., Ferraro, F.R., Fusi Pecci, F., Rich, R.M. & Dalessandro, E. 2010, ApJ, 718, 522
Pancino, E. 2003, PhD Thesis, University of Bologna (P03)
Pancino, E., Ferraro, F.R., Bellazzini, M., Piotto, G. & Zoccali, M. 2004, ApJ, 534, L83
Peterson, R.C. 1981, ApJ, 248, L31
Peterson, R.C. 1982, ApJ, 258, 499
Reimers, D. 1975a, in *Problems in Stellar Atmospheres and Envelopes*, ed. B. Baschek, W.H. Kegel, & G. Traving (Berlin: Springer), 229
Reimers, D. 1975b, Mem. Soc. R. Sci. Liege, 8, 369
Rood, R.T. 1973, ApJ, 184, 815
Smith, G.H., Wood, P.R., Faulkner, D.J. & Wright, A.E. 1990, ApJ, 353, 168
Smith, G.H., Dupree, A.K. & Churchill, C.W. 1992, AJ, 104, 2005
Smith, G.H. & Dupree, A.K. 1998, AJ, 116, 931
Smith, G.H., Dupree, A.K. &+ Strader, J. 2004, PASP, 116, 819

Sollima, A., Ferraro, F.R., Origlia, L., Pancino, E. & Bellazzini, M. 2004, A&A, 420, 173
Sollima, A., Ferraro, F.R., Pancino, E. & Bellazzini, M. 2005a, MNRAS, 357, 265
Sollima, A., Pancino, E., Ferraro, F.R., Bellazzini, M., Straniero, O. & Pasquini, L. 2005b, ApJ, 634, 332
Vieytes, M., Mauas, P.J.D. & Cincunegui, C. 2005, A&A, 441, 701
Vieytes, M., Mauas, P.J.D. & Daz, R.F. 2009, MNRAS, 398, 1495